

Received July 31, 2020, accepted August 4, 2020, date of publication August 6, 2020, date of current version August 19, 2020.

Digital Object Identifier 10.1109/ACCESS.2020.3014817

# Influence of Geometry of Metallic Nanoparticles on Absorption of Thin-Film Organic Solar Cells: A Critical Examination

LONG QIAN CAO<sup>1</sup>, ZI HE<sup>1</sup>, (Member, IEEE), WEI E. I. SHA<sup>2</sup>, (Senior Member, IEEE), AND RU-SHAN CHEN<sup>1</sup>, (Senior Member, IEEE)

<sup>1</sup>Communication Engineering Department, Nanjing University of Science and Technology, Nanjing 210094, China

<sup>2</sup>Key Laboratory of Micro-nano Electronic Devices and Smart Systems of Zhejiang Province, Zhejiang University, Zhejiang 310027, China

Corresponding author: Zi He (zihe@njjust.edu.cn)

This work was supported in part by the Natural Science Foundation of under Grant 61890541 and Grant 61701232, in part by the Jiangsu Province Natural Science Foundation under Grant BK20170854, and in part by Thousand Talents Program for Distinguished Young Scholars of China under Grant 588020-X01801/009.

**ABSTRACT** Well-engineered light trapping designs will significantly improve power conversion efficiency of thin-film organic solar cells. Recently, metallic nanoparticles (NPs) have been widely used to concentrate sunlight in the active layer of OSCs. To critically examine the influence of geometry of metallic NPs on absorption of OSCs, the parallel finite-element method is applied to simulate the near-field multiple scattering effects in plasmonic NPs incorporated OSCs. The geometry-varied NPs including nano-cone, nano-inverted-cone, nano-cylinder, and nano-cuboid are systematically investigated. Furthermore, the absorption enhancement from the dielectric silicon NPs and perfectly reflecting NPs are also comprehensively offered. Compared to the off-plasmon resonance case, the absorption enhancement factor is higher for on-plasmon resonance case. However, the absorption of organic active material near plasmon resonance weakly contributes to exciton generation. Moreover, the height-dependent Fabry-Perot mode plays a key role in the light trapping off the plasmon resonance. Additionally, the tapered structure of the silver nano-cone, which leads to the best absorption enhancement of 3 at the wavelength of 680 nm, since it can reduce unwanted reflection loss and achieve broadband plasmonic resonance simultaneously.

**INDEX TERMS** Plasmonic effect, organic solar cell, metallic nanoparticles, finite-element method.

## I. INTRODUCTION

Thin-film organic solar cells (OSC) have a great potential to generate electrical energy as a renewable energy source [1], [2]. In recent years, the research of organic solar cells has made great progress, and the photoelectric conversion efficiency has been constantly improved. The material of active layer plays a key role in improving power conversion efficiency. P3HT:PCBM is a good candidate for active layer because of its low cost and environmental sustainability. However, compared with the conventional inorganic or perovskite solar cells, the PCE for OPV devices should be further improved. The conflict between the need of thick active layer to ensure sufficient photon absorption and maintaining thin film due to the relatively low carrier mobility

and short exciton diffusion length of organic materials is one of the main obstacles for the efficiency enhancement. More specifically, the absorption of OSCs have been enhanced [4] by metallic nanoparticles (NPs), which excite localized plasmonic resonances (LPRs) [5] and trap the light at the active layer [6], [7]. Since silver (Ag) NPs, in contrast to gold ones, typically can have a larger spectral overlap with absorption region of organic materials in the visible light region, and thus exhibit better improvements of short-circuit current ( $J_{sc}$ ) and power conversion efficiency (PCE) [8]–[10]. Besides metallic nanoparticles (NPs), adopting periodic plasmonic structures is also an efficient approach to enhance optical absorption [11], [12]. The absorption efficiencies of OSCs embedded with the plasmonic NPs are comprehensively studied by using various numerical modeling techniques [13]–[17]. The near-field multiple scattering effects were investigated in [13] for both the active and

The associate editor coordinating the review of this manuscript and approving it for publication was Ladislav Matekovits.

carrier transporting layers. Then the two-dimensional finite-element method (FEM) [2] was adopted to analyze light absorption in [14]. Moreover, metallic NPs with different geometries, such as spherical Ag nanoparticles and triangular Ag nanoprisms, are incorporated in OSCs to improve the power conversion efficiency (PCE) [15]. However, all the previous results and conclusions did not separate the contribution of plasmon resonance with other resonance mechanisms for boosting optical absorption of OSCs. The absorption enhancement comparisons between different geometries and materials have not been examined critically to unveil wave physics to achieve state-of-the-art light-trapping design based on NPs.

On the other hand, more efficient full-wave numerical solution to the optical response of high-performance photovoltaics are urgently required. A lot of three-dimensional numerical methods have been proposed to model the electromagnetic problems, such as scattering [18], [19], radiation [20], [21], electronic device modeling [22] and OSCs [14], [23]–[25], [27]. Because of huge computational resources and ill-conditioned matrix, it is tremendously challenging to design and optimize plasmonic OSCs by using the full-wave numerical methods. For the finite-difference frequency-domain (FDFD) [23] and finite-difference time-domain (FDTD) [26] methods, the rectangular meshes result in staircase errors, thus it is difficult to simulate the metallic NPs with high precision. More specifically, a lot of Lorentz-Drude terms are needed to fit the permittivity of dispersive materials for the time-domain methods, which leads to tremendous computing workload. Moreover, for the finite-element boundary-integral (FE-BI) method, the convergence is bad because of the ill-conditioned matrix. Finally, for the surface integral equation method [22], the fast algorithm is hard to be implemented. Therefore, the frequency-domain finite-element method (FEM) is more attractive than the above-mentioned numerical methods to model optical properties of OSCs.

In this work, the three-dimensional finite-element method is used to rigorously solve the Maxwell's equations. All the simulations are taken by our own codes, which has been verified by other softwares. By using the tetrahedron meshes, metallic NPs with curved interfaces can be precisely modeled. Furthermore, the Floquet boundary condition is utilized to model the OSC device, where the distance between NPs are well separated to avoid degrading electrical properties of devices. In this way, only a unit cell needs to be calculated and the computational resources can be significantly saved. Additionally, the parallel technique is introduced to further accelerate the calculation. All the simulations are taken in visible light regime ranging from 400 to 800 nm. We theoretically investigate shape-dependent absorption of OSCs by appropriately manipulating the geometries of metallic NPs. To systematically examine the geometry-dependent plasmon resonance and meanwhile fairly compare the absorption enhancement between different NPs-embedded OSCs, four kinds of metallic shapes (nano-cone, nano-inverted-cone,

nano-cylinder, and nano-cuboid) are modeled with the same volume (metal amounts). The work is critically important for designing and optimizing NPs-embedded thin-film solar cells.

The reminder of the paper is organized as follows: Section 2 presents the theory of the periodic finite-element method (p-FEM). Section 3 demonstrates the efficiency of the proposed method and study the dependence of light absorption on the shape of the NPs. Finally, a conclusion is presented in Section 4.

## II. THEORY AND FORMULATION

In this section, the wave equation is formulated in terms of the scattered electric field form, which can be written as

$$\nabla \times \nabla \times \mathbf{E}^s - \varepsilon_r k_0^2 \mathbf{E}^s = (\varepsilon_r - 1) \varepsilon_0 \omega^2 \mathbf{E}^i \quad (1)$$

where  $\mathbf{E}^s$  is the scattered electric field,  $\mathbf{E}^i$  is the incident electric field, and the position-dependent permittivity in inhomogeneous solar cell structure is  $\varepsilon_0 \varepsilon_r(\mathbf{r})$ .

Then, as shown in Fig.1, The spacer layers is PEDOT:PSS and the active layer is P3HT:PCBM, Ag Nps is embed in the active layer, the top layer is TiO<sub>2</sub> cathode and the bottom layer is metallic anode [30]. Meanwhile, the periodic boundary conditions are imposed to the OSC unit cell, and Sunlight is regarded as plane waves.

$$\begin{aligned} \mathbf{E}_R &= \mathbf{E}_L e^{-jk_y P} \\ \mathbf{E}_B &= \mathbf{E}_F e^{-jm_k x P} \\ \mathbf{E}_{C_3} &= \mathbf{E}_{C_1} e^{-jP(mk_x + nk_y)} \\ \mathbf{E}_{C_4} &= \mathbf{E}_{C_2} e^{-jP(mk_x - nk_y)} \\ \mathbf{E}_R &= \mathbf{E}_L e^{-jk_y P} \\ \mathbf{E}_B &= \mathbf{E}_F e^{-jm_k x P} \end{aligned} \quad (2)$$

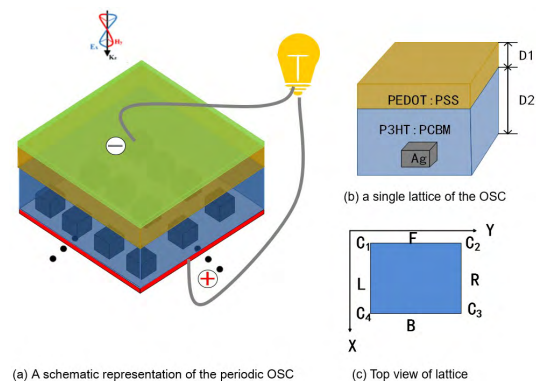


**FIGURE 1.** The schematic of the plasmonic OSC. (a) A schematic representation of the periodic OSC. The spacer layers is PEDOT:PSS and the active layer is P3HT:PCBM. The bandgap and density of states for the active layer are 1.1eV and  $2.5 \times 10^{19} \text{cm}^{-3}$  respectively. The green one is TiO<sub>2</sub> cathode layer has an injection barrier of 0.2eV, the red one is metallic anode layer assumed to be an ohmic contact. The NPs are embedded in the active layer. (b) A single lattice of the OSC. The geometric size of the OSC cell is  $P \times P \times D_1$  for the PEDOT:PSS domain,  $P \times P \times D_2$  for the P3HT:PCBM domain. (c) Top view of the OSC cell. B, F, L, R represent the back, front, left and right sides of the OSC cell. C1, C2, C3, and C4 are the corners.

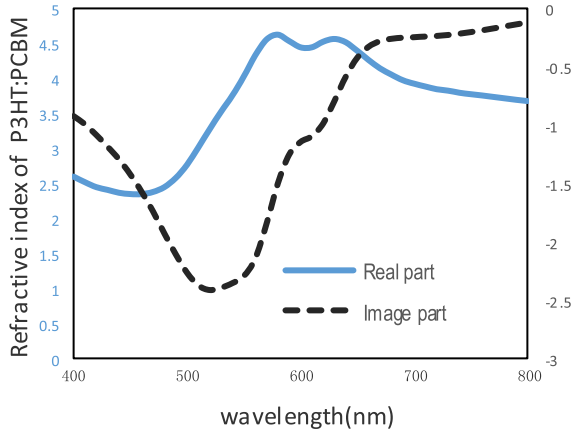


FIGURE 2. The complex refractive index of active layer P3HT:PCBM.

$$\begin{aligned} \mathbf{E}_{C_3} &= \mathbf{E}_{C_1} e^{-jP(mk_x + nk_y)} \\ \mathbf{E}_{C_4} &= \mathbf{E}_{C_2} e^{-jP(mk_x - nk_y)} \end{aligned} \quad (3)$$

where  $k_x, k_y$  are the propagation constants of plane waves along the  $x$  and  $y$  directions,  $m, n$  represent the number of the unit cells along the  $x$  and  $y$  directions.

### III. NUMERICAL RESULTS

The light absorption enhancement and Generation is defined as

$$EF = \frac{\int_{v_{PCBM} - v_{Ag}} |\mathbf{E}_{Ag}(\lambda, \mathbf{r})|^2 dv}{\int_{v_{PCBM}} |\mathbf{E}(\lambda, \mathbf{r})|^2 dv} \quad (4)$$

$$G(r, \lambda) = \int_{400nm}^{800nm} \frac{2\pi}{h} n_r(\lambda), k_i(\lambda) \epsilon_0 |E(r, \lambda)|^2 \Gamma(\lambda) d\lambda \quad (5)$$

where  $\lambda$  is the incident wavelength,  $\mathbf{E}_{Ag}$  represents the electric field at the active layer when the Ag NPs are embedded in active layer,  $\mathbf{E}$  donates the electric field at the active layer without Ag NPs,  $h$  is the Planck constant,  $n_c = n_r + ik_i$  is the complex refractive index of the active material, as shown in figure 2. And  $\Gamma$  is the solar irradiance spectrum for AM 1.5G power of  $100 \text{ mW} \cdot \text{cm}^{-2}$  to simulate the harvesting of sunlight at outdoor. It is worthy of noticing that the absorption of silver regions have been excluded and only active material absorption is taken into account. The common material of P3HT:PCBM is commercially available for active layer due to the complexity of the polymer chemistry, materials science, device engineering, and device physics involved [3].

At first, we consider the influence of NP materials on the absorption enhancement for the cubical geometry shape with  $P = 80 \text{ nm}$ . The thickness of the active layer is  $D_2 = 80 \text{ nm}$  and that of the spacer layer is  $D_1 = 20 \text{ nm}$ . In this numerical example, three kinds of materials (Ag, Silicon, and perfect electric conductor) are used to comparatively study the absorption enhancement. The addition of Ag NPs into the active layer significantly enhances carrier mobility but decreases the total extracted carrier. The designed structure ensures the carrier collection efficiency by controlling the weight ratio for Ag NPs in the active layer by [31]. The sizes of NPs is  $P_A = D_3 = 27.15 \text{ nm}$ . As shown in Fig. 3, the absorption spectra of the OSC are demonstrated as a function of wavelengths for metallic NPs. It can be found that the

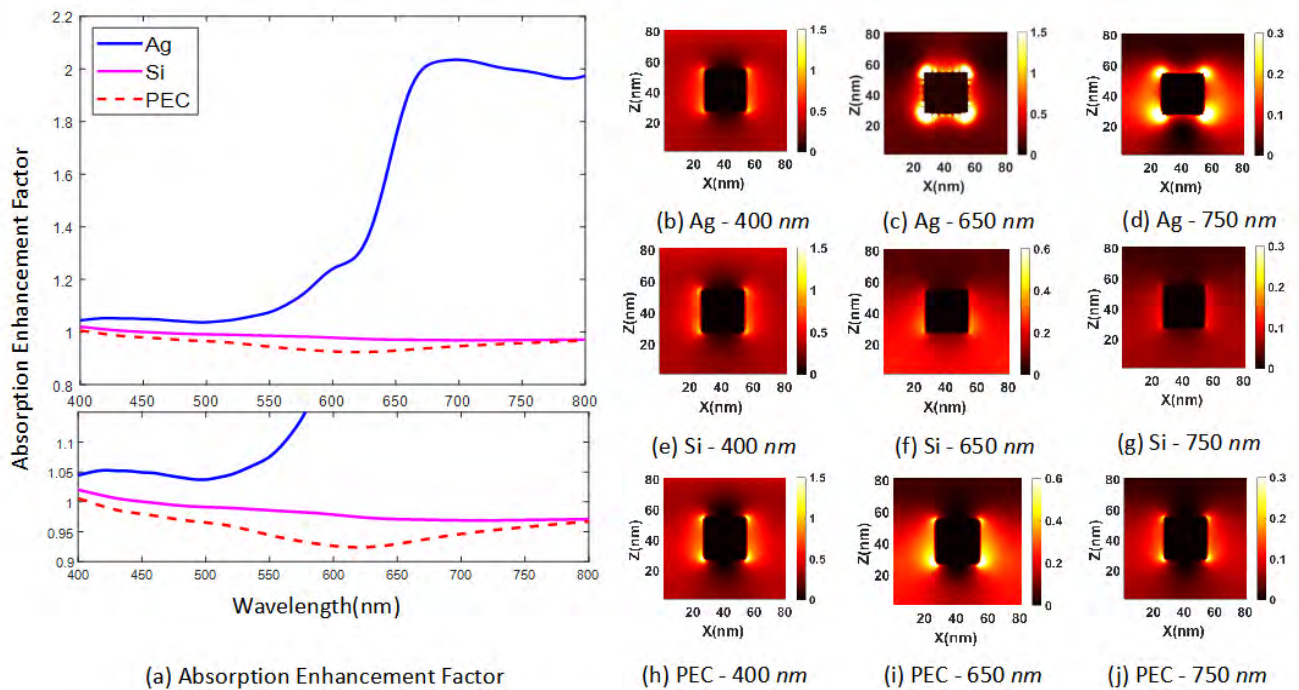


FIGURE 3. (a) Absorption enhancement for different NPs materials. The absorption is calculated only from the P3HT:PCBM active material. Absorption profiles of active layer for different NPs materials: (b-d) Ag; (e-g) Si; (h-j) PEC.

plasmonic enhancement are strongest due to the concentrated E-field around the metallic NPs. More specifically, the largest absorption enhancement factor can be obtained at the wavelength of 750 nm and it is up to 2. However, the absorption enhancement factor for PEC NPs as perfect reflectors is smaller than one since all the Sunlight energy is reflected back from the metal surface to air. Similarly, for Si NPs, the absorption enhancement factor is near to one since its size is too small to allow for resonance (with small scattering cross section). Moreover, incorporating large dielectric NPs into very thin active layer ( $\sim 100$  nm) is not practical for OSCs. Additionally, the material-dependent absorption profiles at the active layer are illustrated in Fig.3 with the wavelength of 400 nm, 650 nm, and 750 nm. At 400 nm, metallic NPs show weak plasmonic enhancement and large reflection can be observed as that in PEC material (perfect reflector) and silicon. As the wavelengths become longer and longer, plasmonic near-field enhancement around the Ag cubes, together with hot spots at the corners due to the lightning rod effect, can be clearly observed compared to other materials. Furthermore, we found that Ag NPs always achieve the best absorption enhancement (in contrast to other materials based NPs) no matter which geometries (cuboid, cylinder, cone, inverted-cone) are adopted. As shown in Fig. 4, the parallel efficiency is tested for 4, 8, 16 and 32 CPU cores respectively and it can be defined as follows.

$$E_P = \frac{1}{N} \cdot \frac{S_1}{S_N} \quad (6)$$

in which  $N$  is the number of cores,  $S_1$  represents the simulation time for one core,  $S_N$  denotes the simulation time by using  $N$  cores. As the core number increases, the decreasing rate of parallel efficiency is noticeably reduced and the parallel efficiency tends to be stable, which suggests the FEM method developed is suitable for large-scale solar cell modeling.

Then the generation rates of the OSCs are theoretically simulated for nano-cone, nano-cylinder, nano-cuboid and nano-inverted-cone. It should be noted that the volume (metal amounts) of the Ag NPs remains unchanged for all the geometries. Firstly, for all the geometries, the excitons are dominantly generated from Sunlight illumination ranging from 400 nm to 650 nm, which is off plasmon resonance after comparing Fig. 5 (off plasmon resonances) to Fig. 6 (on plasmon resonances). For off-resonance cases at Fig. 5, the enhanced generation rates are gained by the height-dependent Fabry-Perot modes and there are the three peaks around 48 nm, 60 nm, 72 nm, which are identical for all NPs. Moreover, the largest generation rate can be obtained for nano-cone because of its tapered structure, which easily achieves impedance matching and reduced unwanted reflection. This argument could be reconfirmed by the worst absorption obtained by the nano-inverted-cone. It can be concluded that the capability of trapping light is enhanced significantly for this scheme. On the other hand, the localized surface plasmon mode is excited for the long wavelengths

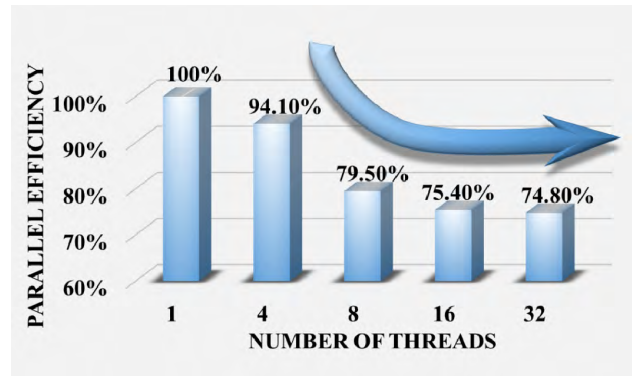


FIGURE 4. Parallel efficiency demonstration by FEM method.

ranging from 650 nm to 800 nm as depicted in Fig. 6. The plasmon resonance has a bad spectral overlap with the absorption region of P3HT:PCBM. Because the strong active material absorption will damp the intensity of plasmon resonance [28]. As the height of Ag NPs increases, the geometric cross section of NPs (projection area at the xoy plane) decreases, which causes weak plasmonic absorption. The best generation rates is again achieved by nano-cone and it shows a broad-band enhancement from short to high altitudes. Consequently, it can be concluded that the Ag NP of nano-cone is the best concentrator from short wavelengths to long wavelengths. To further clarify the wave physics for the long-wavelength enhancement, the generation rate for a three-dimensional nano-cylinder (left y-axis) and the total scattering width for the corresponding two-dimensional nano-cylinder embedded in the P3HT:PCBM (right y-axis) are comparatively studied in terms of different radius. The total scattering width can be defined as

$$\sigma(\lambda) = \frac{4}{k_0} \int_0^{2\pi} \left| \sum_{-\infty}^{+\infty} a_n e^{jn\varphi} \right|^2 d\varphi \quad (7)$$

$$a_n = \frac{\eta_1 J_n(k_0 a) J_n'(k_1 a) - \eta_0 J_n(k_1 a) J_n'(k_0 a)}{\eta_0 J_n(k_1 a) H_n^{(2)'}(k_0 a) - \eta_1 J_n'(k_1 a) H_n^{(2)}(k_0 a)} \quad (8)$$

where  $a$  denote the radius of the 2D cylinder.

As shown in Fig. 7, two peaks correspond to the radius of 18.6 nm (height of 55 nm for the three dimensional nano-cylinder) and 17.1 nm (height of 65 nm for the three dimensional nano-cylinder). The peak positions of total scattering width of the 2D cylinder agree well with those of generation rate of the 3D cylinder, which suggests that plasmonic mode contributes to the improved absorption of OSCs at longer wavelengths. More interestingly, the enhancement peaks of nano-cone NPs have significant shifts compared to those of other NPs (See Fig. 6). Regarding the nano-cone NPs, the positions of enhancement peaks keep unchanged if one observes Figs. 6 and 7 together. These peaks are related to the vertical Fabry-Perot resonance of the nano-cone. Moreover, broadband plasmon resonances induced by the continuously changed cross sections make the peaks broaden. Thus, the hybrid Fabry-Perot-plasmon mode of the nano-cone



TABLE 1. Comparison of the maximum absorption enhancement factor for different geometries.

Geometry	Maximum Absorption Enhancement Factor
Nano-Cone	3.1
Nano-Cuboid	1.6
Nano-Cylinder	1.3
Nano-Inverted-Cone	0.9
Nano-Particles	1.2
Nano-prisms	1.2
Nano-Particles + Nano-prisms	1.3

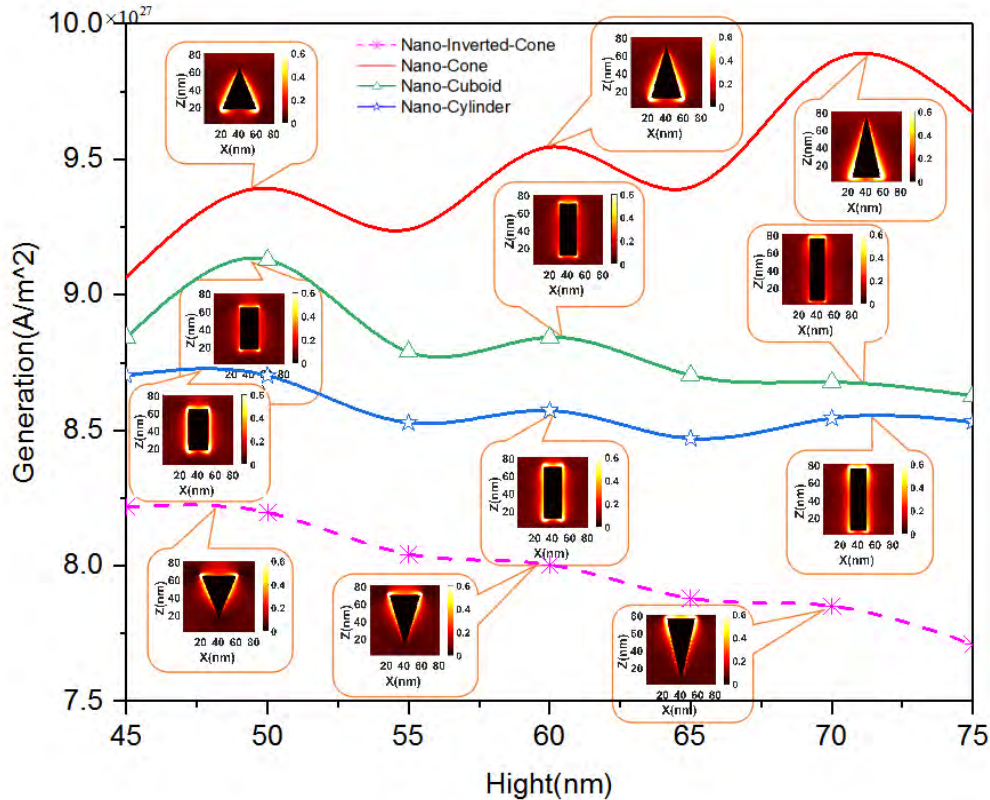
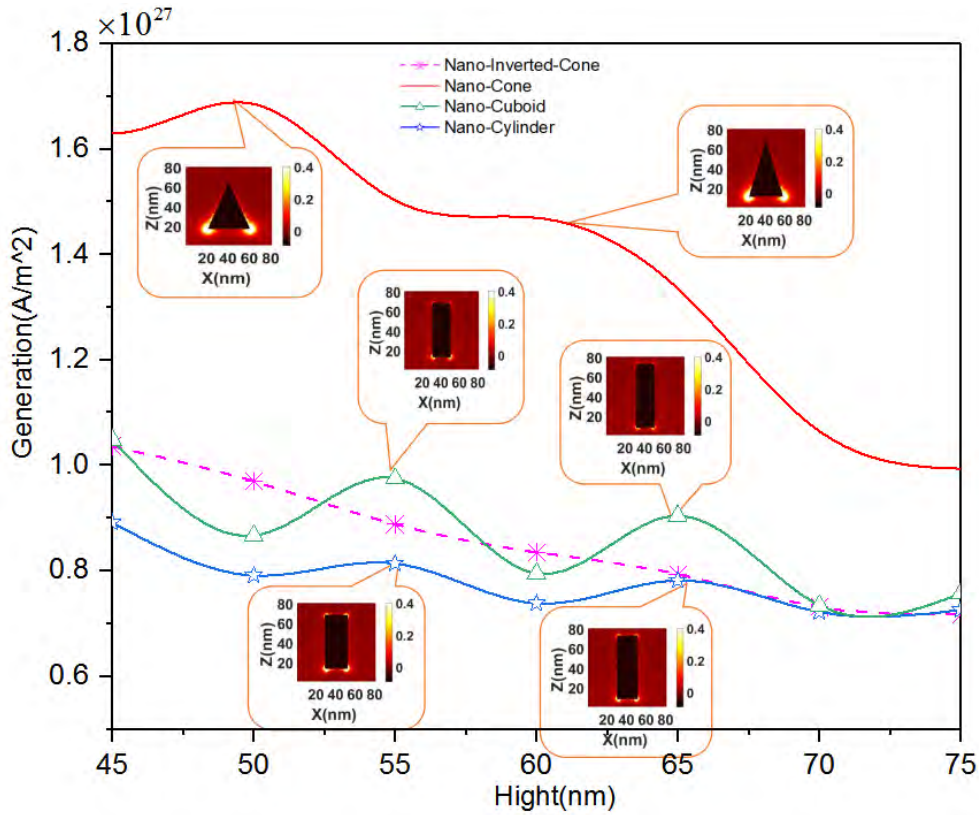


FIGURE 5. Generation rates for different geometrical NPs. For all the geometries, the excitons are dominantly generated from Sunlight illumination ranging from 400 nm to 650 nm, which is off plasmon resonance. The enhanced generation rates are gained by the height-dependent Fabry-Perot modes and there are the three peaks around 48 nm, 60 nm, 72 nm, which are identical for all NPs.

NPs is responsible for the absorption enhancement at longer wavelengths.





To investigate the light trapping cases in details, the wavelength-dependent enhancement factors are illustrated

in Figs. 8-10 for three different heights configurations. The absorption enhancement factor has a peak no matter what shape is embedded in the active layer. The shape of nano-cone performs best among them for all the heights at any



**FIGURE 6.** Generation rates for different geometrical NPs. For all the geometries, the excitons are dominantly generated from Sunlight illumination ranging from 650 nm to 800 nm, which is on plasmon resonance. The localized surface plasmon mode is excited for the long wavelengths ranging from 650 nm to 800 nm.

**TABLE 2.** Comparison for different geometries.

				
Generation( $A / m^2$ )	$9.8 \times 10^{27}$	$8.7 \times 10^{27}$	$9.2 \times 10^{27}$	$8.2 \times 10^{27}$
Absorption Enhancement Factor	3.1	1.2	1.6	0.9
Broadband properties	Yes	No	No	No
Manufacture process	Not easy	Moderate	Easy	Not easy
Overall performance	★★★★★	★★	★★★★	★

wavelength. It can also be concluded that the distribution of the near-field at the wavelength of 660 nm is strongest (Figs. b-m of 8-10). The strongest near-field enhancement is always achieved by the plasmon mode at the resonating wavelength of about 660 nm. Despite the large metallic loss for the Ag NPs, the plasmon mode greatly boosts the near-field

electric field resonating in the active layer. The best choice of height for NPs is 48 nm, which can gain the maximum absorption enhancement factor.

Comparisons of the maximum absorption enhancement factor for different geometries are made in Table 1. The maximum absorption enhancement factor of Nano-Cone

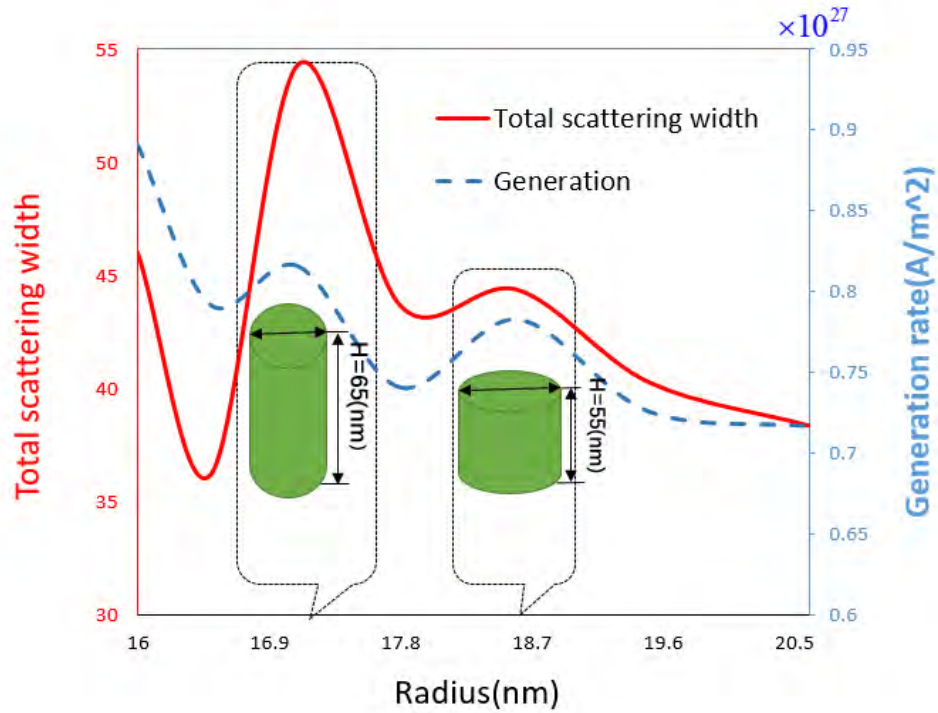


**FIGURE 7.** Generation rates for the nano-cylinder NPs (left y-axis) and total scattering width for the corresponding two-dimensional nano-cylinder embedded in the P3HT:PCBM (right y-axis). There are two peaks related to the radius of 18.6 nm (height of 55 nm) and 17.1 nm (height of 65 nm). The positions of peaks agree well with each other for these two case.

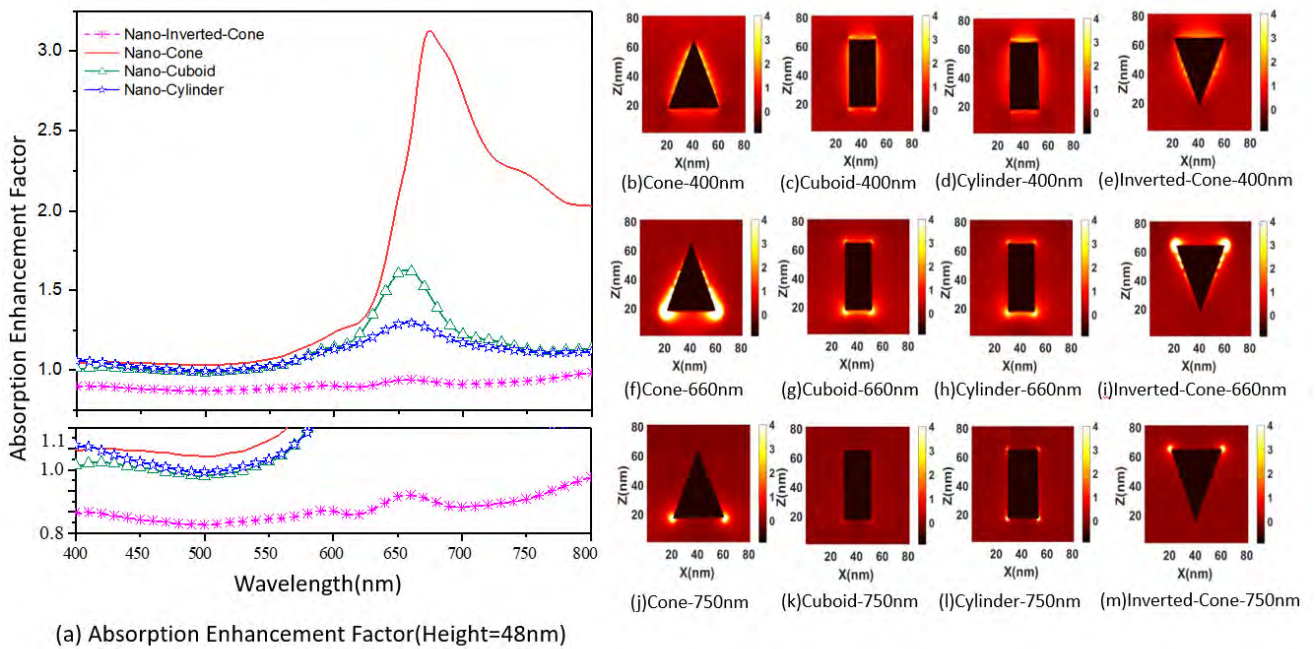


**FIGURE 8.** (a) Absorption enhancement for geometry-dependent NPs for the height of 48 nm. The absorption is calculated only from the P3HT:PCBM active material. Absorption profiles of active layer for different geometrical NPs: (b-e) 400 nm; (f-i) 660 nm; (j-m) 750 nm.

NPs is up to 3, which is superior to the other geometries. The performance for four kinds of NPs geometries are

compared in Table 2. It can be concluded that the nano-cone performs best for generation, absorption enhancement factor



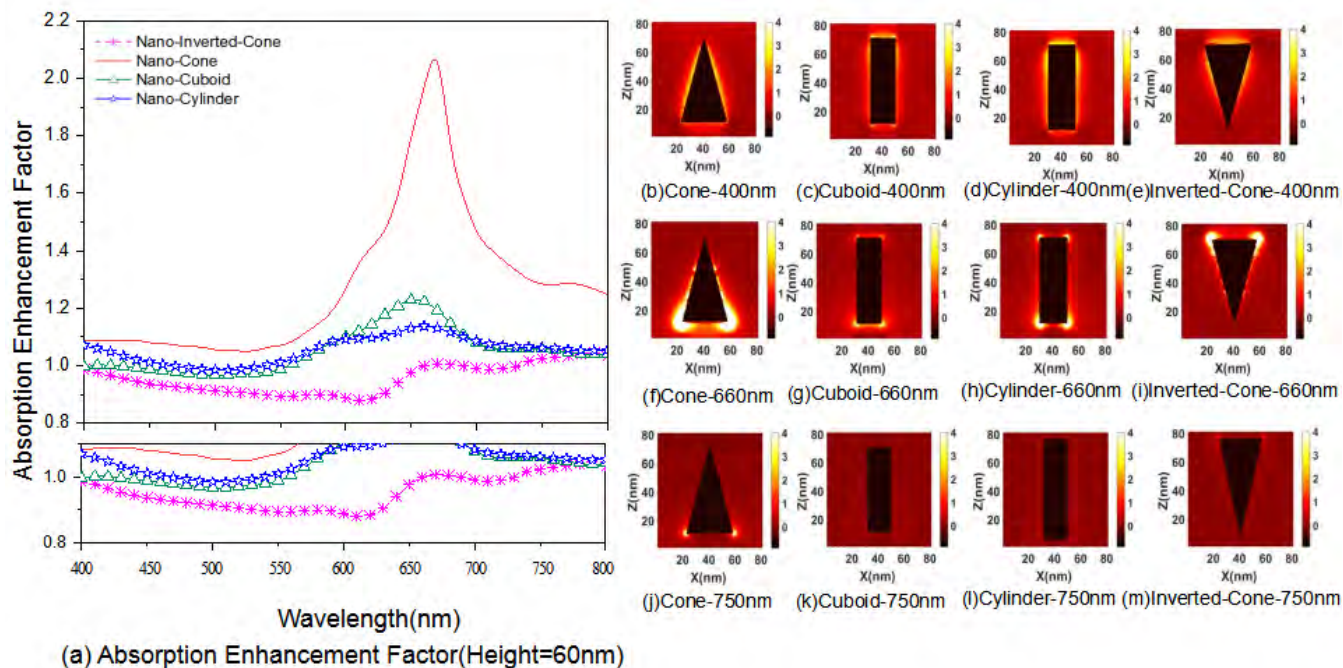


**FIGURE 9.** (a) Absorption enhancement for geometry-dependent NPs for the height of 60 nm. The absorption is calculated only from the P3HT:PCBM active material. Absorption profiles of active layer for different geometrical NPs: (b-e) 400 nm; (f-i) 660 nm; (j-m) 750 nm.

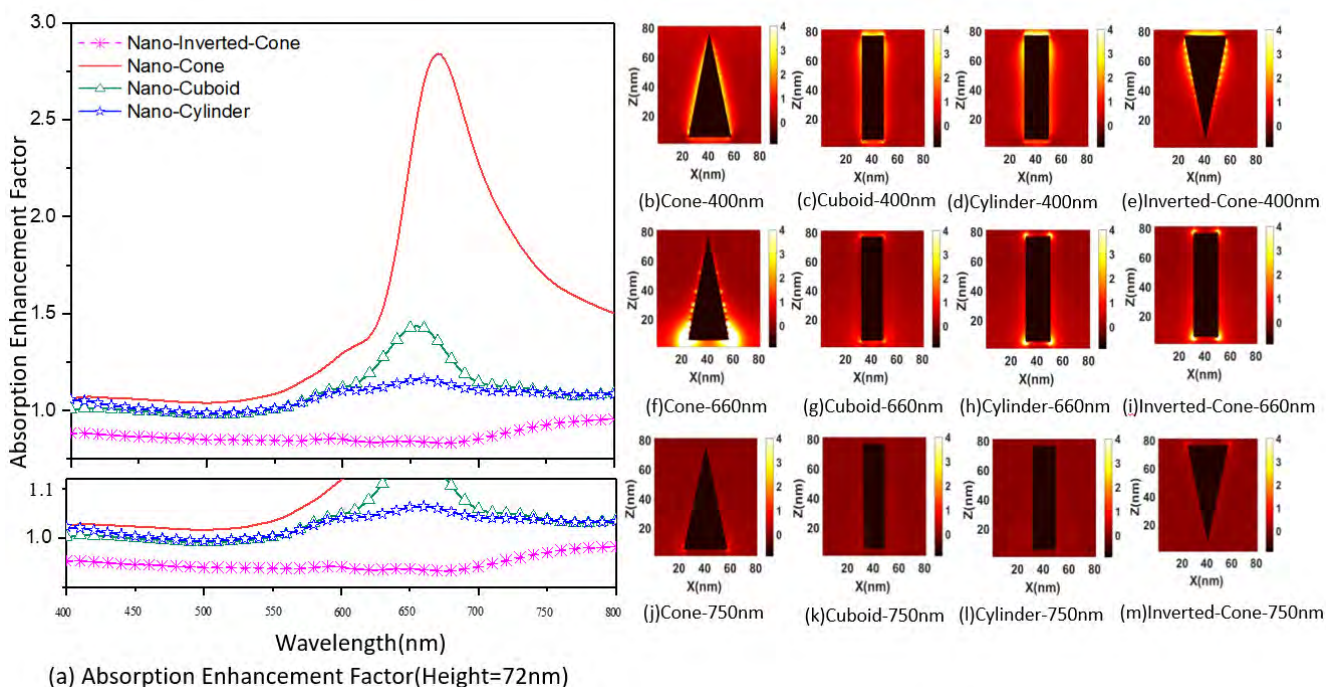


**FIGURE 10.** (a) Absorption enhancement for geometry-dependent NPs for the height of 72 nm. The absorption is calculated only from the P3HT:PCBM active material. Absorption profiles of active layer for different geometrical NPs: (b-e) 400 nm; (f-i) 660 nm; (j-m) 750 nm.

and broadband properties. In other words, it can significantly improve the utilization of solar radiation energy from short-wavelength to long-wavelength.

**IV. CONCLUSION**

A parallel finite-element method is presented to simulate thin-film plasmonic OSCs. Numerical examples show



the material-dependent, cross section-dependent height-dependent, and shape-dependent near-field light-trapping effects by various NPs. We found that Fabry-Perot mode induced enhancement is dominant from 400 nm to 650 nm and the plasmonic mode induced enhancement is dominated from 650 nm to 800 nm. All in all, the Ag NPs of nano-cone exhibit the highest optical absorption from short wavelengths to long wavelengths. It can be concluded from the numerical results that the highest absorption enhancement factor for the silver nano-cone can be up to 3 at the wavelength of 680 nm. The tapered structure of Ag nano-cone not only reduces undesired reflection from active layer (gains good impedance matching) but also supports broadband plasmonic enhancement. It should be noted that the simple and low-cost manufacturing technology of wet chemical synthesis can be applied to realize these tapered structures. Our work offers efficient mathematical approach and deep physical understanding to design and optimize high-efficiency OSCs.

## REFERENCES

- [1] X. Li, W. C. H. Choy, L. Huo, F. Xie, W. E. I. Sha, B. Ding, X. Guo, Y. Li, J. Hou, J. You, and Y. Yang, "Dual plasmonic nanostructures for high performance inverted organic solar cells," *Adv. Mater.*, vol. 24, no. 22, pp. 3046–3052, 2012.
- [2] D. M. Solís, J. M. Taboada, F. Obelleiro, L. M. Liz-Marzán, and F. J. G. de Abajo, "Toward ultimate nanoplasmonics modeling," *ACS Nano*, vol. 8, no. 8, pp. 7559–7570, Aug. 2014.
- [3] M. T. Dang, L. Hirsch, and G. Wantz, "P3HT:PCBM, best seller in polymer photovoltaic research," *Adv. Mater.*, vol. 23, no. 31, pp. 3597–3602, Aug. 2011.
- [4] J. Yuan, Y. Zhang, L. Zhou, G. Zhang, H.-L. Yip, T.-K. Lau, X. Lu, C. Zhu, H. Peng, P. A. Johnson, M. Leclerc, Y. Cao, J. Ulanski, Y. Li, and Y. Zou, "Single-junction organic solar cell with over 15% efficiency using fused-ring acceptor with electron-deficient core," *Joule*, vol. 3, no. 4, pp. 1140–1151, Apr. 2019.
- [5] M. Zhu, Y. Li, F. Chen, X. Zhu, J. Dai, Y. Li, Z. Yang, X. Yan, J. Song, Y. Wang, E. Hitz, W. Luo, M. Lu, B. Yang, and L. Hu, "Plasmonic wood for high-efficiency solar steam generation," *Adv. Energy Mater.*, vol. 8, no. 4, 2018, Art. no. 1701028.
- [6] M. Kobylko, P.-E. Coulon, A. Slablab, A. Fafin, J. Cardin, C. Dufour, A. Losquin, M. Kociak, I. Monnet, D. Mailly, X. Lafosse, C. Ulysse, E. Garcia-Caurel, and G. Rizza, "Localized plasmonic resonances of prolate nanoparticles in a symmetric environment: Experimental verification of the accuracy of numerical and analytical models," *Phys. Rev. A, Gen. Phys.*, vol. 9, no. 6, Jun. 2018, Art. no. 064038.
- [7] J. Yang, Q. Sun, K. Ueno, X. Shi, T. Oshikiri, H. Misawa, and Q. Gong, "Manipulation of the dephasing time by strong coupling between localized and propagating surface plasmon modes," *Nature Commun.*, vol. 9, no. 1, pp. 1–8, Dec. 2018.
- [8] X. Chen, B. Jia, J. K. Saha, B. Cai, N. Stokes, Q. Qiao, Y. Wang, Z. Shi, and M. Gu, "Broadband enhancement in thin-film amorphous silicon solar cells enabled by nucleated silver nanoparticles," *Nano Lett.*, vol. 12, no. 5, pp. 2187–2192, May 2012.
- [9] S.-S. Kim, S.-I. Na, J. Jo, D.-Y. Kim, and Y.-C. Nah, "Plasmon enhanced performance of organic solar cells using electrodeposited Ag nanoparticles," *Appl. Phys. Lett.*, vol. 93, no. 7, Aug. 2008, Art. no. 073307.
- [10] D. H. Wang, K. H. Park, J. H. Seo, J. Seifter, J. H. Jeon, J. K. Kim, J. H. Park, O. O. Park, and A. J. Heeger, "Enhanced power conversion efficiency in PCDTBT/PC70BM bulk heterojunction photovoltaic devices with embedded silver nanoparticle clusters," *Adv. Energy Mater.*, vol. 1, no. 5, pp. 766–770, Oct. 2011.
- [11] C. Min, J. Li, G. Veronis, J.-Y. Lee, S. Fan, and P. Peumans, "Enhancement of optical absorption in thin-film organic solar cells through the excitation of plasmonic modes in metallic gratings," *Appl. Phys. Lett.*, vol. 96, no. 13, Mar. 2010, Art. no. 133302.
- [12] A. Abass, H. Shen, P. Bienstman, and B. Maes, "Angle insensitive enhancement of organic solar cells using metallic gratings," *J. Appl. Phys.*, vol. 109, no. 2, Jan. 2011, Art. no. 023111.
- [13] W. E. I. Sha, W. C. H. Choy, Y. G. Liu, and W. C. Chew, "Near-field multiple scattering effects of plasmonic nanospheres embedded into thin-film organic solar cells," *Appl. Phys. Lett.*, vol. 99, no. 11, Sep. 2011, Art. no. 113304.
- [14] K. Q. Le, A. Abass, B. Maes, P. Bienstman, and A. Alù, "Comparing plasmonic and dielectric gratings for absorption enhancement in thin-film organic solar cells," *Opt. Express*, vol. 20, no. 1, pp. 39–50, 2012.
- [15] X. Li, W. C. H. Choy, H. Lu, W. E. I. Sha, and A. H. P. Ho, "Efficiency enhancement of organic solar cells by using shape-dependent broadband plasmonic absorption in metallic nanoparticles," *Adv. Funct. Mater.*, vol. 23, no. 21, pp. 2728–2735, Jun. 2013.
- [16] K. Chan, M. Wright, N. Elumalai, A. Uddin, and S. Pillai, "Plasmonics in organic and perovskite solar cells: Optical and electrical effects," *Adv. Opt. Mater.*, vol. 5, no. 6, Mar. 2017, Art. no. 1600698.
- [17] Z. Huang, L. Cheng, B. Wu, and X. Wu, "The study of optical and electrical properties of solar cells with oblique incidence," *IEEE Photon. Technol. Lett.*, vol. 28, no. 19, pp. 2047–2049, Oct. 1, 2016.
- [18] J. M. Song and W. C. Chew, "Multilevel fast-multipole algorithm for solving combined field integral equations of electromagnetic scattering," *Microw. Opt. Technol. Lett.*, vol. 10, no. 1, pp. 14–19, Sep. 1995.
- [19] Z. He and R. S. Chen, "A novel parallel parabolic equation method for electromagnetic scatterings," *IEEE Trans. Antennas Propag.*, vol. 64, no. 11, pp. 4777–4784, Nov. 2016.
- [20] Y. Lo and S. Lee, "A study of space-tapered arrays," *IEEE Trans. Antennas Propag.*, vol. 14, no. 1, pp. 22–30, Jan. 1966.
- [21] P. Gu, G. Wang, Z. Fan, and R. Chen, "Efficient unitary matrix pencil method for synthesising wideband frequency patterns of sparse linear arrays," *IET Microw., Antennas Propag.*, vol. 12, no. 12, pp. 1871–1876, Oct. 2018.
- [22] S. Chen, D. Ding, and R. Chen, "Time-domain impulse response with the TD-VSIE field-circuit coupling algorithm for nonlinear analysis of microwave amplifier," *IEEE Microw. Wireless Compon. Lett.*, vol. 28, no. 5, pp. 431–433, May 2018.
- [23] C. P. Yu and H. C. Chang, "Compact finite-difference frequency-domain method for the analysis of two dimensional photonic crystals," *Opt. Express*, vol. 12, no. 7, pp. 1397–1408, 2004.
- [24] R. S. Kim, J. Zhu, J. H. Park, L. Li, Z. Yu, H. Shen, M. Xue, K. L. Wang, G. Park, T. J. Anderson, and Q. Pei, "E-beam deposited Ag-nanoparticles plasmonic organic solar cell and its absorption enhancement analysis using FDTD-based cylindrical nano-particle optical model," *Opt. Express*, vol. 20, no. 12, p. 12649, Jun. 2012.
- [25] S. He, W. E. I. Sha, L. Jiang, W. C. H. Choy, W. C. Chew, and Z. Nie, "Finite-element-based generalized impedance boundary condition for modeling plasmonic nanostructures," *IEEE Trans. Nanotechnol.*, vol. 11, no. 2, pp. 336–345, Mar. 2012.
- [26] W. E. I. Sha, W. C. H. Choy, and W. C. Chew, "A comprehensive study for the plasmonic thin-film solar cell with periodic structure," *Opt. Express*, vol. 18, no. 6, pp. 5993–6007, 2010.
- [27] Z. He, J. H. Gu, W. E. I. Sha, and R. S. Chen, "An efficient volumetric method of moments for modeling plasmonic thin-film solar cells with periodic structures," *Opt. Express*, vol. 26, no. 19, pp. 25037–25046, 2018.
- [28] Y. H. Jang, Y. J. Jang, S. Kim, L. N. Quan, K. Chung, and D. H. Kim, "Plasmonic solar cells: From rational design to mechanism overview," *Chem. Rev.*, vol. 116, no. 24, pp. 14982–15034, Dec. 2016.
- [29] S. Guo, L. Yang, Y. Zhang, Z. Huang, X. Ren, W. E. I. Sha, and X. Li, "Enhanced hydrogen evolution via interlaced Ni<sub>3</sub>S<sub>2</sub>/MoS<sub>2</sub> heterojunction photocatalysts with efficient interfacial contact and broadband absorption," *J. Alloys Compounds*, vol. 749, pp. 473–480, Jun. 2018.
- [30] A. K. Kang, M. H. Zandi, and N. E. Gorji, "Fabrication and degradation analysis of perovskite solar cells with graphene reduced oxide as hole transporting layer," *J. Electron. Mater.*, vol. 49, no. 3, pp. 2289–2295, Mar. 2020.
- [31] M. Xue, L. Li, B. J. T. de Villiers, H. Shen, J. Zhu, Z. Yu, A. Z. Stieg, Q. Pei, B. J. Schwartz, and K. L. Wang, "Charge-carrier dynamics in hybrid plasmonic organic solar cells with Ag nanoparticles," *Appl. Phys. Lett.*, vol. 98, no. 25, p. 119, 2011.



**LONG QIAN CAO** was born in Anhui, China. He received the B.Sc. degree in electronic information science and technology from the Department of Information Engineering, West Anhui University, Luan, China, in 2018. He is currently pursuing the master's degree with the Nanjing University of Science and Technology.



**ZI HE** (Member, IEEE) was born in Hebei, China. She received the B.Sc. and Ph.D. degrees in electronic information engineering from the School of Electrical Engineering and Optical Technique, Nanjing University of Science and Technology, Nanjing, China, in 2011 and 2016, respectively. She has worked as a Visiting Scholar with the University of Illinois, Urbana and Champaign (UIUC), from September 2015 to September 2016.

She works as a Postdoctoral with the Science and Technology on Electromagnetic Scattering Laboratory, BIEF. Since 2019, she has been an Associate Professor with the Department of Communication Engineering, Nanjing University of Science and Technology. Her research interests include antenna, RF-integrated circuits, and computational electromagnetics.



**WEI E. I. SHA** (Senior Member, IEEE) received the B.S. and Ph.D. degrees in electronic engineering from Anhui University, Hefei, China, in 2003 and 2008, respectively. From July 2008 to July 2017, he was a Postdoctoral Research Fellow and then a Research Assistant Professor with the Department of Electrical and Electronic Engineering, University of Hong Kong, Hong Kong. From March 2018 to March 2019, he worked at University College London as a Marie Skłodowska-Curie

Individual Fellow. Since October 2017, he joined the College of Information Science and Electronic Engineering, Zhejiang University, Hangzhou, China, where he is currently a tenure-tracked Assistant Professor. He has authored or coauthored 136 refereed journal articles, 121 conference publications (including 31 invited talks), five book chapters, and two books. His research interests include theoretical and computational research in electromagnetics and optics, focusing on the multiphysics and interdisciplinary research. His research involves fundamental and applied aspects in computational and

applied electromagnetics, nonlinear and quantum electromagnetics, micro- and nano-optics, optoelectronic device simulation, and multiphysics modeling. His Google Scholar citation is 5378 with H-index of 34. He is a member of OSA. He served as a Reviewer for 50 technical journals and a Technical Program Committee Member of nine IEEE conferences. In 2015, he was awarded the Second Prize of Science and Technology from Anhui Province Government, China. In 2007, he was awarded the Thousand Talents Program for Distinguished Young Scholars of China. He has also received five best student paper prizes and one Young Scientist Award with his students. He also served as an Associate Editor for *Progress in Electromagnetics Research*, IEEE ACCESS, and the IEEE OPEN JOURNAL OF ANTENNAS AND PROPAGATION, and a Guest Editor for the IEEE JOURNAL ON MULTISCALE AND MULTIPHYSICS COMPUTATIONAL TECHNIQUES and *The Applied Computational Electromagnetics Society Journal*.



**RU-SHAN CHEN** (Senior Member, IEEE) was born in Jiangsu, China. He received the B.Sc. and M.Sc. degrees from the Department of Radio Engineering, Southeast University, China, in 1987 and 1990, respectively, and the Ph.D. degree from the Department of Electronic Engineering, City University of Hong Kong, in 2001. He joined the Department of Electrical Engineering, Nanjing University of Science and Technology (NJUST), China, where he became a Teaching Assistant

in 1990 and a Lecturer in 1992. Since September 1996, he has been a Visiting Scholar with the Department of Electronic Engineering, City University of Hong Kong, first as Research Associate, then as a Senior Research Associate in July 1997, a Research Fellow in April 1998, and a Senior Research Fellow in 1999. From June to September 1999, he was also a Visiting Scholar with Montreal University, Canada. In September 1999, he was promoted to Full Professor and Associate Director of the Microwave and Communication Research Center in NJUST, and in 2007, he was appointed as the Head of the Department of Communication Engineering, NJUST. He was appointed as the Dean in the School of Communication and Information Engineering, Nanjing Post and Communications University, in 2009. And in 2011 he was appointed as Vice Dean of the School of Electrical Engineering and Optical Technique, NJUST. Currently, he is a principal investigator of more than ten national projects. His research interests mainly include computational electromagnetics, microwave integrated circuit and nonlinear theory, smart antenna in communications and radar engineering, microwave material and measurement, and RF-integrated circuits. He has authored or coauthored more than 260 articles, including over 180 articles in international journals.

• • •